Hygrothermal characterization of cement mortar composites incorporating micronized miscanthus fibers

Franck Komi Gbekou, Ferhat Benmahiddine, Abderrahim Boudenne, Rafik Belarbi, Anissa Eddhahak, Karim Benzarti

Case Studies in Construction Materials 21 (2024) e04004

Contents lists available at ScienceDirect

Case Studies in Construction Materials

journal homepage: www.elsevier.com/locate/cscm

Hygrothermal characterization of cement mortar composites incorporating micronized miscanthus fibers

Franck Komi Gbekou [a], Ferhat Benmahiddine [b], Abderrahim Boudenne [c], Rafik Belarbi [d], Anissa Eddhahak [e], Karim Benzarti [a,*]

[a] Univ Gustave Eiffel, Ecole des Ponts, CNRS, Navier, Marne-la-Vallée F-77447, France
[b] ESTP, Institut de Recherche, Cachan F-94230, France
[c] Univ Paris-Est Créteil, CERTES, Créteil F-94010, France
[d] La Rochelle University, LaSIE, UMR 7356 CNRS, La Rochelle F-17042 CEDEX 1, France
[e] Arts et Métiers ParisTech, Laboratoire Procédés et Ingénierie en Mécanique et Matériaux (PIMM), Paris F-75013, France

ARTICLE INFO

Keywords:
Bio-based mortar
Micronized miscanthus fibers
Thermal and hygric properties
Moisture content
Sorption isotherm
MBV
Capillary absorption
GAB model

ABSTRACT

This work investigates both the moisture dependence of thermal properties and the hygric behavior of cement mortars incorporating different proportions of micronized miscanthus fibers up to ~7 wt%. The experimental program encompasses thermal characterization at dry (10 % RH), moderate (50 % RH), and saturated (100 % RH) states of samples, along with hygric characterization of the various mortar specimens through sorption-desorption tests, water vapor permeability assessment, Moisture Buffer value (MBV) determination, and capillary absorption tests. Thermal measurements showed a significant decrease in thermal conductivity with the addition of fibers. For a given biobased mortar composition, conductivity values were almost identical at dry/moderate RH level but exhibited an increase at saturation. This shift was attributed to the fibers' absorptive properties, which lead to a higher water content within the samples in saturated humidity environments. Collectively, the moisture sorption, moisture buffering capacities, water vapor permeability, and capillary absorption properties demonstrated consistent enhancement with rising fiber content, confirming the significant impact of plant fibers on the material's hygrothermal properties. In addition, the GAB model (Guggenheim- Anderson-de Boer) was used to fit the sorption and desorption isotherms, yielding a good correspondence with experimental data. Finally, mortars with the higher fiber contents (M7.5 F and M10F with 5.70 wt% and 6.94 wt% of fibers, respectively) combined high hygroscopicity and low thermal conductivity values (even under moisture-saturated conditions), making them promising candidates for applications requiring both good hygric performance and effective insulation properties.

1. Introduction

The building industry is responsible for approximately 30 % of energy consumption and CO_2 emissions, making it one of the most significant contributors to environmental degradation and global warming [1,2]. Traditional building materials, such as concrete and cement, require vast amounts of natural resources, which leads to environmental depletion, pollution, and waste emissions.

* Corresponding author.
E-mail addresses: fbenmahiddine@estp.fr (F. Benmahiddine), boudenne@u-pec.fr (A. Boudenne), rbelarbi@univ-lr.fr (R. Belarbi), Anissa.EDDHAHAK@ensam.eu (A. Eddhahak), karim.benzarti@univ-eiffel.fr (K. Benzarti).

https://doi.org/10.1016/j.cscm.2024.e04004
Received 10 June 2024; Received in revised form 21 October 2024; Accepted 18 November 2024
Available online 19 November 2024

In this context, bio-based building materials have gained considerable attention over the last decade, due to their potential to effectively mitigate the environmental impact of the construction industry. By incorporating agricultural by-products or wastes into conventional building materials, bio-based alternatives not only minimize primary resource consumption but also impart enhanced performance characteristics to the resulting composites [3–5]. This dual advantage has positioned bio-based building materials as an attractive option for sustainable construction practices, addressing both environmental and functional requirements.

Plant materials, including hemp, flax, rice husk, cork, date palm fibers, among others, have been widely investigated for their potential applications in construction. One prominent benefit of incorporating these plant fibers into cement mortars or concrete is the creation of ultra-lightweight materials with substantial enhancements in thermal performance, particularly through a notable reduction in thermal conductivity. This effect can be attributed to two main factors: the inherently low thermal conductivity of the plant fibers themselves and the overall increase in porosity observed in the resulting biobased composites [6–12]. For instance, Boumhaout et al. [7] observed a remarkable 70 % improvement in the thermal resistance of mortars containing date palm fibers. Horma et al. also demonstrated a reduction in thermal conductivity from 0.62 to 0.2 $W.m^{-1}.K^{-1}$ by incorporating 10 wt% spent tea into a cement mortar [8]

In addition, bio-based building materials generally offer excellent hygric properties that contribute to their moisture regulation capacity, enabling them to moderate fluctuations in relative humidity and maintain optimal indoor air quality [12]. The high intrinsic microporosity of the cellulose-rich component in plant fibers facilitates the rapid absorption and release of moisture in response to environmental changes. This characteristic plays a crucial role in ensuring a comfortable indoor environment within the building.

Several crucial material properties are indicative of this moisture-regulation capacity, including the Moisture Buffer Value (MBV), water vapor permeability, and sorption/desorption characteristics.

The Moisture Buffer Value denotes the capacity of a material to store/release moisture when subjected to repeated fluctuations in relative humidity. According to the NordTest classification [13,14], MBV values exceeding 2 $g.m^{-2}.\%RH^{-1}$ are considered indicative of excellent moisture regulators. Such elevated values are frequently observed in the literature for biobased mortars. For example, Charai et al. [6] achieved moisture buffering capacities of 2.29 and 3.13 $g.m^{-2}.\%RH^{-1}$ by adding 5 and 10 wt% Alfa fibers to a cement-based mortar. Chennouf et al. also documented a MBV of 2.97 $g.m^{-2}.\%RH^{-1}$ for a bio-based mortar containing 15 wt% date palm fibers [15]. Additionally, Benmahiddine et al. reported a MBV of 2.27 $g.m^{-2}.\%RH^{-1}$ for hemp concrete with 16 % hemp shives [9]. This indicates that the incorporation of these vegetal fibers significantly enhances the material's capacity to buffer moisture, contributing to a stable and comfortable indoor environment.

Moreover, this moisture regulation capability can also be highlighted through the adsorption/desorption isotherms of the material [15]. Indeed, incorporating vegetative aggregates into a cementitious matrix leads to an increase in the maximum adsorbed water content. This can be attributed to the sensitivity of vegetal aggregates to moisture. Their incorporation into construction materials results in a material with a greater capacity for both adsorption and desorption. Consequently, in the event of excess humidity in the living environment, the material can absorb the moisture and release it back into the indoor environment when needed, thereby facilitating natural humidity regulation.

Furthermore, the inclusion of plant fibers in cement mortars also enhances water vapor permeability, facilitating efficient vapor transportation across the material's thickness. Chennouf et al. [15] found water vapor permeability values of 3.16×10^{-11} and 3.59×10^{-11} $kg.m^{-1}.s^{-1}.Pa^{-1}$ in dry and wet cup tests, respectively, for mortars containing 15 wt% date palm fibers. Brás et al. [16] noted a 20 % increase in water vapor permeability with the incorporation of 70 % cork by volume in cement mortar composites.

Because biobased materials exhibit strong hygroscopic tendencies, fluctuations in moisture content resulting from environmental changes can also influence their thermal properties. Indeed, numerous studies have highlighted the dependence of thermal properties on moisture content. For instance, Gourlay et al. [17] observed an increase in thermal conductivity of hemp concrete with increasing water content. Similarly, Pierre et al. [18] reported a roughly 1.5-fold increase in thermal conductivity for hemp concrete at 95 % relative humidity compared to its dry state (approximately 0 % humidity). Overall, thermal conductivity increases with water content [17,19,20]. As water fills the pores of the mortar, its higher thermal conductivity compared to air enhances heat transfer by shifting the dominant mechanism from natural convection to conduction within the pores. Hence, it is imperative to explore thermal and hygric properties in a closely interconnected manner.

This study is part of a broader project aiming to enhance the mechanical and thermo-hydric performance of cement mortars by incorporating phase change materials or micronized vegetal fibers, with the goal of developing building envelope materials that offer improved thermal efficiency and moisture management [21–24]. The selection of fibers derived from the miscanthus plant (x giganteus) is motivated by its substantial potential for utilization, characterized by impressive annual productivity (10–20 tons/year), adaptability to diverse soil conditions, and minimal water and fertilization demands, making it a highly attractive choice [25–28]. In France, this plant is primarily grown in the northern region, where concerted efforts are being made to establish an industrial-level valorization chain.

In a preliminary phase of the study, we examined the effects of adding micronized miscanthus fiber (up to 6.94 wt%) to cement mortar composites, focusing on microstructure, mechanics, and thermal properties [22]. The results demonstrated that the adopted manufacturing protocol effectively ensures a homogeneous dispersion of micronized fibers within the mortars, thereby imparting macroscopically isotropic properties to the resulting composites. Additionally, the biobased mortars exhibited a significant increase in thermal resistance after fiber addition, with an 87 % reduction in thermal conductivity (from 2.34 to 0.4 $W\cdot m^{-1}\cdot K^{-1}$), primarily due to increased porosity. However, this enhancement came at the cost of reduced mechanical strength due to increased porosity content and weak bonding between vegetal fibers and the mineral matrix, making these bio-based mortars unsuitable for structural applications but still adequate for handling and insulation in construction.

In this paper, we explore the moisture-dependent thermal properties and hygric behavior of the same cement composites with

varying concentrations of micronized miscanthus fibers up to approximately 7 wt%. The experimental program covers thermal characterization under dry, moderate, and saturated conditions, as well as hygric characterization, encompassing the assessment of moisture buffer value, water vapor permeability, sorption/desorption behavior, and capillary absorption. Furthermore, a theoretical approach based on the GAB model (Guggenheim-Anderson-de Boer) is also applied to describe the moisture sorption behavior.

Due to the scarcity of literature data on the thermo-hygric properties of construction materials with miscanthus fibers, the present experimental results establish a valuable database for readers. Moreover, these findings offer essential input data for future modeling efforts focused on predicting thermo-hydric behavior at the wall scale.

2. Materials and methods

2.1. Materials and sample preparation

The plant fillers selected in this study consist of a micronized powder of miscanthus fibers, with fiber length in the range of 200–500 μm. This product was supplied by Addiplast Group (Saint-Pal-de-Mons, France) under the reference MDDCH0114 MISCANTHUS 200–500μm/BFF. According to the technical datasheet, the micronization process results in a cellulose content of approximately 94 %, while the hemicellulose and lignin contents are reduced to 6 % and 0.4 %, respectively.

This micronized powder is generally used in the plastic industry to manufacture bio-based fiber-reinforced polymer composites for the automotive market. In the present work, it is proposed to introduce this vegetal filler (as received without any chemical treatment) into a cement mortar, and to evaluate the impact of this addition on the overall thermophysical and hygric properties. Due to their small size and their very porous cellulosic structure (see Fig. 1), these micronized miscanthus particles are expected to develop a higher specific surface area compared to longer chopped fibers, and hence to influence more significantly the properties of the mortar composites. Unfortunately, this study did not include a quantitative assessment of the fiber's intrinsic porosity. However, future work should incorporate an analysis of micropore size distribution using methods such as BJH (Barrett-Joyner-Halenda) analysis or

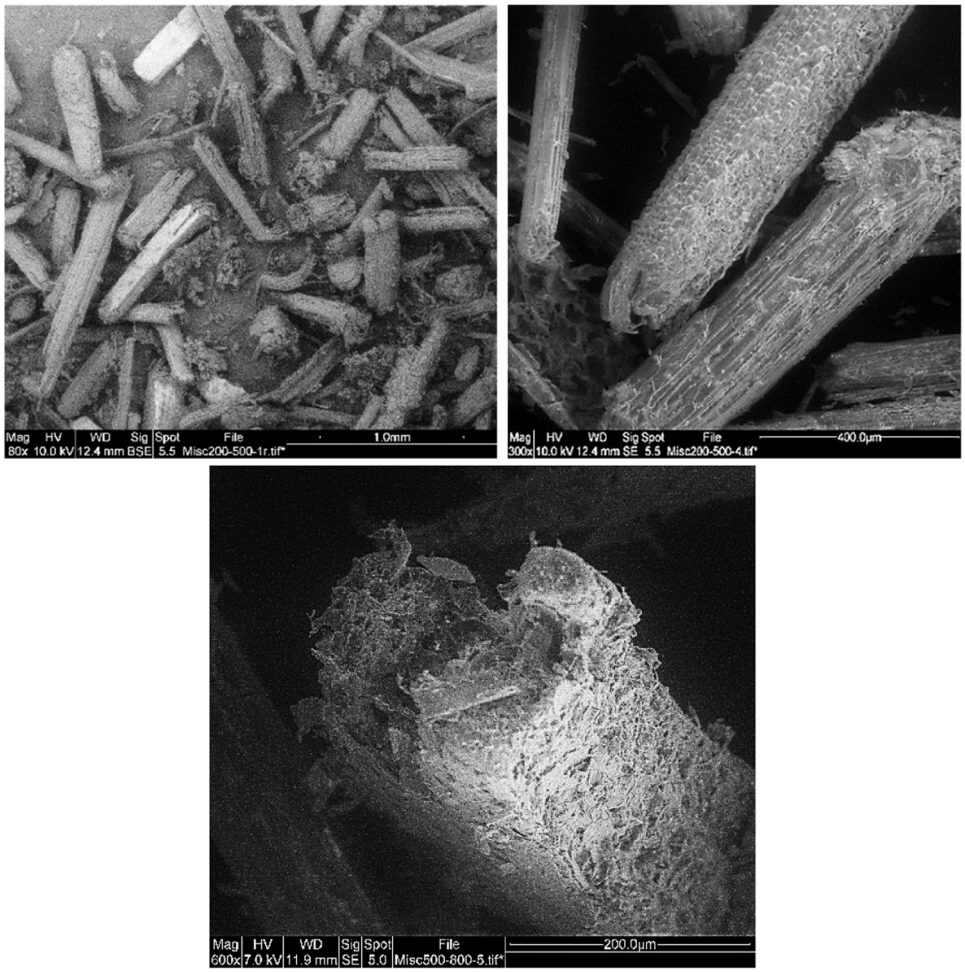

Fig. 1. Scanning Electron Microscopy (SEM) images of the micronized miscanthus fibers at different magnifications.

thermoporosimetry via differential scanning calorimetry (DSC).

Additionally, the use of micronized powder ensures a homogeneous particle distribution within the mortar matrix [22].

A mortar composition available in the literature [29,30] and specifically designed for additive manufacturing was also considered in this work. The selection of this formulation aligns with the broader objective of the project, which aims to develop 3D-printable mortars incorporating vegetal fibers. However, this specific aspect of the project is not addressed in the present paper.

Table 1 presents the details of this reference composition, denoted M0, which is based on a water-to-cement ratio (W/C) of 0.35. Two types of cements were combined in a proportion of 93/7 parts by weight: an Ordinary Portland Cement EXTREMAT® CEM I 52,5 N-SR3 SEG containing 99 % of Clinker (denoted OPC) and a rapid setting Sulfo-aluminous cement Alpenat R^2 (denoted CSA), both manufactured by VICAT company (L'Isle-d'Abeau, France). The role of CSA cement is to accelerate the setting of the fresh mortar mix at an early stage, improving the cohesion of the deposited layers in 3D printing applications. A superplasticizer, namely VISCOCRETE TEMPO 11 from SIKA Company (Baar, Switzerland), was also added to the mix and will be denoted SP in the following. The reference mortar also comprises standardized siliceous sand (granular distribution complying with EN 196–1 standard [31], with a maximum size of 2 mm), which was supplied by SNL company (Leucate, France).

Several mortar admixtures were prepared by introducing various dosages of micronized miscanthus powder in the reference system M0. Their compositions are summarized in Table 1. The amounts of mineral components (OPC/CSA cement, sand) and SP were kept constant in the mixes, while the quantities of miscanthus fibers and water were varied. The different mortar formulations are denoted MxF, where x is the target dosage of miscanthus fibers introduced in the mortar (expressed in wt% of the reference composition M0), which was varied in the range of 0–10 wt%. The actual mass fraction of dry miscanthus fibers in each system (calculated by dividing the mass of dry miscanthus fibers by the total mass of all mortar components, including water) is also displayed in Table 1**.** Additionally, the effective volume content of miscanthus fibers in the fresh mixes was calculated using a skeleton density of 1570 kg/m^3 for the fibers [22] and is also included in the table.

In order to offer the reader an inclusive collection of information, the densities of the different constituent materials, along with the theoretical compositions of the fresh mix expressed in kg.m^{-3}, are additionally presented in the Appendix (Tables A1 and A2, respectively).

It is to note that the amount of water (and hence the W/C ratio) increases together with the fiber content. This is mainly related to the necessity of presoaking the plant fillers in water prior to their incorporation in the mortar mixes. Indeed, preliminary tests showed that the addition of dry fibers led to a drastic reduction in the mortar workability and strongly affected the cement hydration process, since the miscanthus fibers adsorbed a large part of the mixing water (their absorptivity has been reported in the range 390–500 % [32]). In practice, the fibers were presoaked in water for at least 2 hours, in accordance with other authors [33], The excess water was eliminated with a tissue and the soaked fibers were added to the fresh mortar mixes at the end of the mixing process.

The mixing procedure complied with the specifications of EN 196–1 standard and was implemented using a programmable mortar mixer (model E092N from Matest Spa Company, Treviolo, Italy). Further details can be found in [22].

After mixing, the fresh mortars were poured in different molds to manufacture 4 × 4 × 8 cm^3 prismatic samples dedicated to thermophysical characterization, and 4 × 10 × 10 cm^3 samples for hygric characterization. The samples were demolded 24 hours later, hermetically wrapped with a plastic film, and conditioned at (20 ± 1) °C until the characterizations at 28 days.

2.2. Characterization techniques

2.2.1. Characterization of thermophysical properties

Thermophysical properties of the various miscanthus mortars (prims of dimension 4 × 4 × 8 cm^3), were determined using the Hot Disk (HD) method. A Hot Disk TPS 2500 S device (Gothenburg, Sweden) equipped with a Kapton insulated probe (ref 5501 from Hot Disk®, with a radius of 6.4 mm) was used for the measurements. The principle of the HD technique relies on the theory of transient plane source, as specified by ISO 22007–2 standard [34]. The setup uses a sensor placed between two samples of the same material, which acts both as a heat source to increase the temperature at the sample surface, and as a "resistance thermometer" to record the time-dependent temperature increase. The experimental device (Fig. 2) enables simultaneously a rapid, accurate and non-destructive evaluation of the thermal conductivity (noted λ in W.m^{-1}.K^{-1}), the thermal diffusivity (a in m^2.s^{-1}) and the volumetric heat capacity of the sample ($\rho.C_p$ in J.m^{-3}.K^{-1}).

To evaluate the impact of moisture, the thermophysical characteristics of the different mortars were analyzed under three distinct relative humidity (RH) conditions, including dry state (10 % RH), saturated state (close to 100 % RH) and moderate RH level (50 %

Table 1
Composition of the various mortar formulations including micronized miscanthus fibers.

Type of mortar	Sand (g)	OPC (g)	CSA (g)	SP (g)	Dry fibers (g)	Total water* (g)	Water/Cement (OPC+ CSA) ratio	Mass fraction of dry fibers (wt%)	Vol. fraction of dry fibers (vol%)
M0	1350	1059.3	79.7	2.96	-	398.7	0.35	0	0
M2.5 F	1350	1059.3	79.7	2.96	72.3	605.0	0.53	2.28	3.02
M5F	1350	1059.3	79.7	2.96	144.5	843.6	0.74	4.15	5.09
M7.5F	1350	1059.3	79.7	2.96	216.8	1093.0	0.96	5.70	6.56
M10F	1350	1059.3	79.7	2.96	289.1	1383.9	1.21	6.94	7.54

* The total water content includes both the initial mixing water and the additional water absorbed by the miscanthus fibers during the presoaking stage.

RH). Notably, the 10 % RH level was the lowest moisture value permitted by the climatic chamber and was thus considered the dry condition.

In practice, the samples were first placed in a climatic chamber and conditioned at 20°C - 50 % RH until their mass reached an equilibrium state. Thermophysical measurements were then performed inside the chamber at various temperatures between 15°C and 45°C. Once this initial stage was completed, the same samples were reconditioned at 20°C - 10 % RH for at least one week before conducting thermophysical measurements between 15°C and 45°C in this dry state. Finally, for saturated-state measurements (100 % RH), the samples were removed from the chamber and directly immersed in water for a period of one day. Afterward, the excess water was soaked up using a tissue and the samples were reinstalled in the climatic chamber at 90 % RH to perform thermophysical characterizations over the 15–45°C temperature range. Experimental values were averaged on three repeated measurements (performed at different locations of the same conditioned specimen) and uncertainties were derived from the standard deviations.

2.2.2. Moisture buffer value

The Moisture Buffer Value (MBV) of a building material represents its capacity to store and release moisture when exposed to repeated fluctuations in relative humidity between two predefined levels. It serves as a useful indicator for comparing the hygroscopic properties of different materials. However, MBV alone does not fully describe the actual hygric mitigation under service conditions, which also depends on factors such as ventilation, room dimensions, and other environmental variables.

The MBV was determined following the NordTest protocol [13,14]. Samples measuring 10 × 10 × 4 cm^3 were subjected to cyclic variations in relative humidity, alternating between 75 % RH (high level) and 33 % RH (low level) for 8 and 16 hours, respectively, under isothermal conditions at 23°C. The cycles were repeated until each sample reached a quasi-steady state.

Prior to testing, the samples were stabilized at 23°C and 50 % RH until their mass became constant. To ensure unidirectional (1D) moisture transfer, the samples were sealed with plastic film and aluminum insulation tape on all faces except one (as illustrated in Fig. 3).

In these conditions, the MBV (in kg.(m^2.%RH)$^{-1}$) can be estimated using the following expression:

$$MBV = \frac{\Delta m}{A \times (RH_{high} - RH_{low})} \quad (1)$$

Where, Δm is the mass change during the absorption/desorption phase (kg), A is the exchange area (m^2), RH_{high} (75 %) and RH_{low} (33 %) are the predetermined RH levels.

2.2.3. Assessment of the water vapor permeability

The water vapor permeability characterizes the material ability to transfer moisture (through diffusion, effusion and liquid transfer) under a vapor pressure gradient. It can be determined using the sorption cup method under isothermal condition according to EN ISO 12572 standard [35]. For each mortar composition, measurements were made both with wet and dry cup tests.

In practice, a series of samples dedicated to hygric characterizations (dimensions 4 ×10 x 10 cm^3) was cut with a diamond saw to reduce their thickness to 1.5 cm, in order to accelerate the moisture exchange process and shorten the test duration. This thickness meets the standard requirement of being at least three times, and preferably five times, the largest particle size within the mortar (2 mm in the case of the sand particles used).

These samples were then stored at 23°C – 50 % RH until they reached mass equilibrium. In order to create a 1D moisture flow over

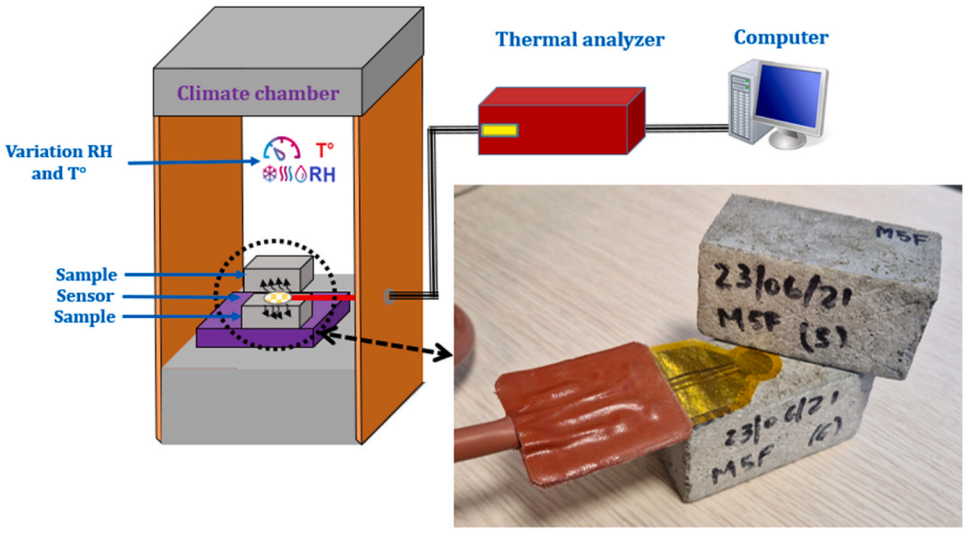

Fig. 2. Experimental setup used to assess the thermophysical properties of mortars over the 15–45°C temperature range and at different RH levels.

Fig. 3. Description of the experimental setup used to evaluate the moisture buffer value.

the 100 cm^2 surface area of the samples, the latter were embedded on the top lid of plastic cups containing specific compounds for moisture control (a saturated potassium sulfate solution was used to maintain 97 % RH in the air layer within the wet cups, while silica gel was used to create a dry condition in the air layer inside the dry cups, with a measured RH value of around 5 %).The plastic cups were made perfectly hermetic by filling the gaps between the samples and the lids with melted wax (see the right image in Fig. 4).

In each cup, the height of the air layer between the silica gel (or the saturated solution) and the lower face of the mortar sample was about 75 mm. Both dry and wet cups were placed in a climatic chamber which was set at 23°C −50 % RH throughout the testing process (Fig. 4).

The cups were weighed every day to record their mass and calculate the water vapor transmission rate in steady-state conditions. The mass change rate G (in $kg.s^{-1}$) between two consecutive measurements was calculated as:

$$G = \frac{\Delta m}{\Delta t} \tag{2}$$

Where Δm and Δt are respectively the mass change (in kg) and laps of time (in s) between successive measurements. The test is stopped and the final value of G is obtained when each of the last five successive determinations of Δm are within ± 5 % of G [35,36].

The water vapor permeance W (in $kg/(m^2 \cdot s \cdot Pa)$) is given by:

$$W = \frac{G}{\Delta P_v A} \tag{3}$$

Where A is the exposed surface area of the sample (m^2) and ΔP_v (Pa) is the water vapor pressure gradient across the sample (difference between the vapor pressure inside the cup and the outer vapor pressure in the climate chamber), which can be calculated using Eq. (4):

$$P_v = RH \times e^{23.5771 - \frac{4042.9}{T - 37.58}} \tag{4}$$

With RH, the relative humidity and T the temperature (in K) [35,36]. The relative humidity in the climate chamber is 50 %, while RH

Fig. 4. Experimental setup for the determination of the water vapor permeability.

levels inside the dry and wet cups are respectively 5 % and 97 %.

The water vapor permeability δ (in kg.m^{-1}.s^{-1}.Pa^{-1}) in the dry and wet cup methods are then calculated using the following formula:

$$\delta = W.d \tag{5}$$

Where d (in m) is the thickness of the mortar sample.

In a subsequent step, water vapor permeability values must be corrected to account for the resistance caused by the air layer in the cup, in accordance with EN ISO 12572.

The measured permeance shall be corrected according to the following formula:

$$W_c = \frac{1}{\frac{A.\Delta P_v}{G} - \frac{d_a}{\delta_a}} \tag{6}$$

Where W_c $(kg/(m^2 \cdot s \cdot Pa))$ is the corrected permeance, d_a (m) is the thickness of the air layer. δ_a (kg.m^{-1}.s^{-1}.Pa^{-1}) represents the water vapor permeability of air, with a value of approximately 2.02×10^{-10} kg/(m·Pa·s), calculated in accordance with the EN ISO 12572 standard assuming an atmospheric pressure of 1013.25 hPa.

The corrected value of the water vapor permeability is finally obtained by:

$$\delta_c = W_c.d \tag{7}$$

In addition, the initial and corrected values of the water vapor resistance factor (μ and μ_c) were also calculated according to:

$$\mu = \frac{\delta_a}{\delta} \text{ and } \mu_c = \frac{\delta_a}{\delta_c} \tag{8}$$

2.2.4. Characterization of the sorption-desorption behavior

The adsorption/desorption isotherms of the different mortars were determined by gravimetric method using a fully automated SPS device from ProUmid Company (Ulm, Germany), equipped with a sample loader (Fig. 5). These experiments were conducted on 1.5 × 1.5 × 1.5 cm^3 cubic samples which were cut from larger specimen. The samples were first preconditioned at 40°C under vacuum until mass stabilization. Afterwards, they were placed in the climatic chamber of the SPS device and exposed to different levels of relative humidity under isothermal condition (23°C). The adsorption/desorption isotherms were constructed from the mass change of the tested specimens (uptake or loss) at equilibrium. Furthermore, the slope of the sorption isotherms (in the adsorption phase) made it possible to determine the moisture storage capacity according to the following expression:

$$C_m = \frac{\partial W}{\partial RH} \tag{9}$$

Where, C_m (adimensional) is the moisture storage capacity and W (%) is the water content of the sample tested.

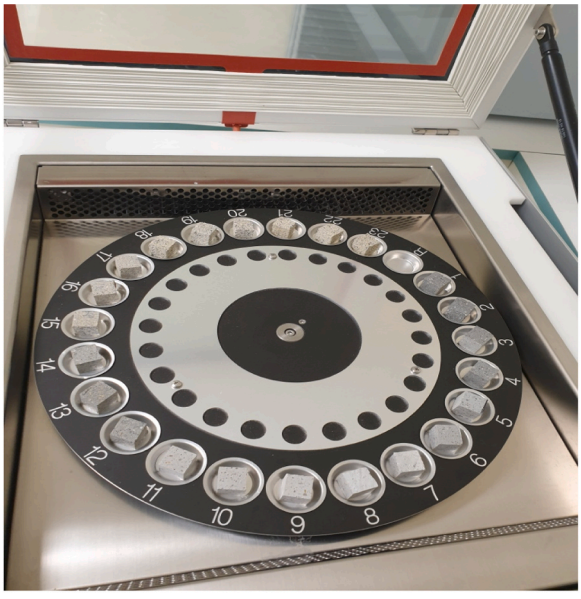

Fig. 5. Gravimetric vapor sorption analyzer (SPS model from ProUmid). Cubic mortar specimens are installed in the auto-sampler.

2.2.5. Assessment of the capillary absorption parameters

The capillary absorption of a material refers to its inherent capacity to spontaneously absorb a liquid without the need for external forces, provided its surface is open and in contact with the liquid. This property is quantified by two key parameters: the capillary absorption coefficient (a) and the capillary moisture content (W_f) of the material. The capillary absorption coefficient denotes the amount of liquid water absorbed per unit area, correlated with the square root of time, while the capillary moisture content represents the maximum liquid water content achievable at saturation within a given volume of the sample.

The capillary behavior is evaluated in accordance with the NF EN 15801 standard [37]. Prior to testing, samples were subjected to drying at 40°C until a constant mass was achieved. The testing procedure involves exposing one face of the sample to water and monitoring the subsequent mass changes until saturation is reached. To ensure unidirectional transfer confined to the exposed surface, all faces of the samples were wrapped in plastic film, except for the bottom surface in contact with the water (refer to Fig. 6). The sample dimensions are approximately 10 × 10 × 5 cm^3, with an exposed area of 10 × 5 cm^2. Mass evolution is tracked using a high-precision balance with 0.1 % accuracy.

The capillary absorption coefficient (a) and the capillary moisture content (W_f) of the material are determined from the recorded data using the following equations:

$$a = \frac{m_h - m_d}{A \times \sqrt{t}} \tag{10}$$

Where: a represents the capillary absorption coefficient (in $kg.m^{-2}.s^{-0.5}$), m_h is the mass of the sample at a specific humidity level (in kg), m_d stands for the dry mass of the sample (in kg), A represents the exposed area of the sample in contact with water (in m^2), and t is the time (s).

$$W_f = \frac{m_{sat} - m_d}{L \times l \times e} \tag{11}$$

Where: W_f represents the capillary moisture content (in $kg.m^{-3}$), m_{sat} denotes the mass of the sample at saturation (measured in kg), L, l and e are the dimensions of the sample (in m)

Note that the drying behavior was not analyzed after sample saturation. The primary objective of this experimental campaign is to determine material properties required as input parameters for heat and mass transfer models. Since the planned modeling work (e.g., using the Künzel model) requires only capillary absorption properties, the drying test was omitted from the program, though it may still be relevant for future studies.

3. Results and discussion

3.1. Summary of previous results from mechanical and microstructural characterization

Previous work involved material-scale characterizations to evaluate various properties of the biobased miscanthus mortars in the

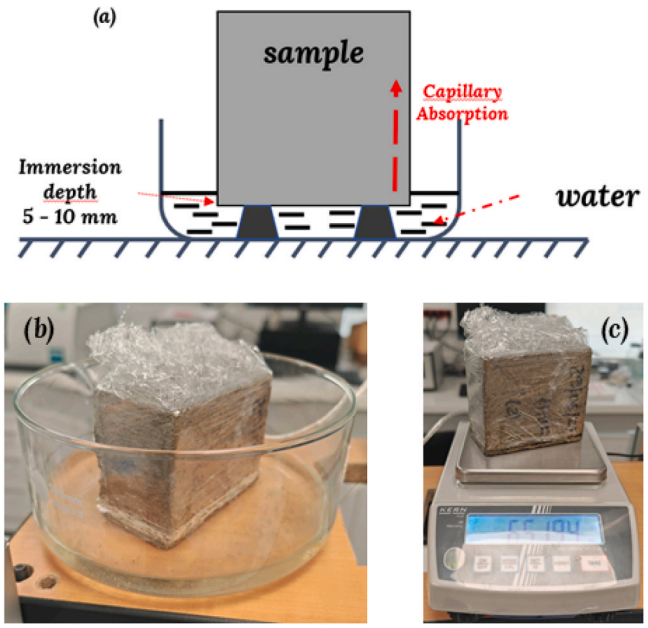

Fig. 6. (a) and (b) Experimental setup used for capillary absorption tests, (c) weighing of the samples with a precision balance.

hardened state, namely:

- Microstructural properties (water-accessible porosity, density) following NF P18–459 standard,
- Mechanical strength at 28 days, in accordance with NF EN 196–1 standard,
- Thermophysical properties (thermal conductivity, thermal diffusivity and heat capacity), measured with the hot-disk method. These properties were assessed only at a constant 50 % RH, whereas the present study considers a broader range of humidity conditions.

Readers are encouraged to consult ref [22] for full details. However, a summary of the key trends is provided in this section to support the interpretations of the findings presented in the following parts of this paper.

Table 2 summarizes the compressive strength, density, and water-accessible porosity of mortars containing varying amounts of micronized miscanthus fibers. In general, increasing the fiber content led to higher porosity and lower density compared to the reference mortar (M0). This behavior was attributed to the intrinsic porosity of the miscanthus fibers and the additional water used to pre-soak the fibers, which evaporates, leaving voids in the microstructure. As a result, the mechanical strength of the biobased mortars decreased significantly.

Additionally, Fig. 7a and b illustrate the thermal conductivity of the studied mortars at 25°C and 50 % RH as a function of density and water-accessible porosity. A clear dependence of thermal conductivity on these two factors was observed. Generally, an increase in porosity (or decrease in density) led to a significant reduction in thermal conductivity. This effect was partly attributed to changes in heat transfer mechanisms, as the air within the pores promotes local thermal transfer through natural convection rather than thermal conduction [10].

3.2. Influence of moisture conditions on thermophysical properties

In the present work, the HD technique was employed to determine the thermophysical properties of the different mortars under varying moisture environments. Measurements were conducted at different controlled relative humidity levels, following the protocol outlined in Section 2.2.1.

Fig. 8 displays the changes in thermal conductivity (λ) of the different mortars across the temperature range of 10–45°C under two conditions - dry-state (at 10 % RH) and water saturation (100 % RH). Similarly, Fig. 9 presents the outcomes related to the changes in thermal diffusivity (α) of the same mortars. The graphs exhibit error bars, which represent standard deviations derived from three repeated measurements.

It is worth noting that the results obtained at intermediate humidity level (50 % RH) were already presented in a prior publication [22] and are not recalled in detail here. However, certain measurements obtained under this condition are employed for comparative purposes.

3.2.1. Findings in dry conditions

Key observations under dry conditions (10 % RH) include:

- The reference mortar M0 exhibited thermal conductivity (λ) and thermal diffusivity (α) values of 2.35 $W.m^{-1}.K^{-1}$ and 1.07 $mm^2.s^{-1}$, respectively at 25°C. These values align with literature data for OPC mortars (λ between 1.5 and 2.7 $W.m^{-1}.K^{-1}$ and α between 0.89–1.26 $mm^2.s^{-1}$, depending on the material's density [38–40]). They are also consistent with findings from Shafigh et al. for mortars of similar density (2200 $kg.m^{-3}$) [38].
- λ for the reference mortar M0 remained almost constant over the temperature range investigated (15–45°C), in accordance with other authors [41].
- Increasing miscanthus fiber content significantly reduced both λ and α. For instance, the mortar with 5.70 wt% fibers had a λ of 0.38 $W.m^{-1}.K^{-1}$, marking an 84 % decrease compared to M0.
- For any given fiber content, λ and α values remained stable across the investigated temperature range, indicating minimal temperature dependence.

This trend of reduced thermal conductivity with increased fiber content also holds at 50 % RH and in saturated moisture conditions. This behavior is consistent with literature findings, where the addition of plant fibers generally enhances mortar thermal resistance. For example, Charai et al. [6] observed reduced thermal conductivity in concrete with increased alfa fiber content, and Salem et al.

Table 2
Summary of mechanical and microstructural characterization results [22].

Type of mortar	Mass fraction of fibers (wt%)	Compressive strength at 28 days (MPa)	Density ($kg.m^{-3}$)	Water accessible porosity (%)
M0	0	72.1	2.32	19.7
M2.5 F	2.28	21	1.93	33.1
M5F	4.15	7.05	1.59	47
M7.5F	5.70	2.41	1.34	57.3
M10F	6.94	0.99	1.19	61.3

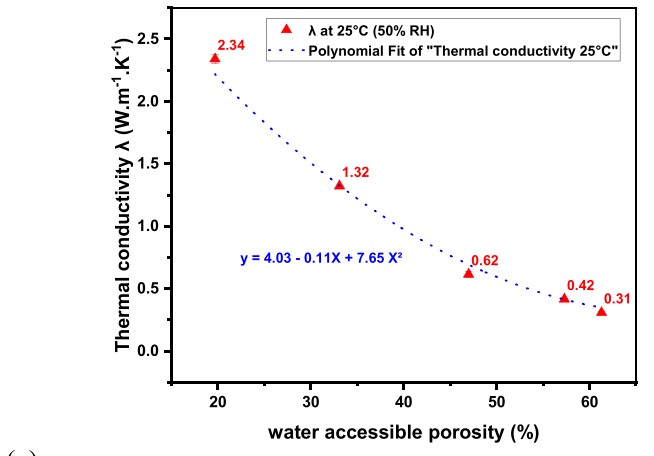

(a)

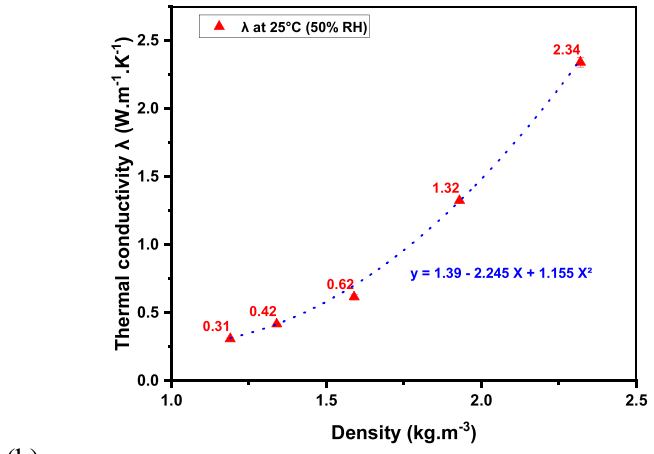

(b)

Fig. 7. Dependence of the thermal conductivity of the biobased mortars at 25°C and 50 % RH upon (a) the water accessible porosity and (b) the density.

[42] noted a 63 % improvement in thermal performance when substituting 20 wt% natural sand with vegetable synthetic sponge waste. Similarly, Benmansour et al. [43] reported a significant thermal conductivity reduction of 87–98 % with 30 % date palm fibers of various sizes in natural cement mortars, while Panesar & Shindman [10] found a marked decrease in concrete thermal conductivity upon adding waste cork.

The observed reduction in thermal conductivity of bio-based mortars can be attributed both to (i) the low thermal conductivity of miscanthus fibers, which measures only 0.04 $W{\cdot}m^{-1}{\cdot}K^{-1}$ [44], and (ii) to the increased overall porosity, which shifts heat transfer mechanisms from conduction to natural convection within the pores [3,6,10,33,42,45,46].

Although miscanthus mortars do not match the insulation performance of materials like insulation wools or loose fill materials (thermal conductivities below 0.1 $W{\cdot}m^{-1}{\cdot}K^{-1}$), they maintain mechanical cohesion, allowing their use as non-load-bearing wall elements. With thermal conductivities between 0.3 and 0.6 $W{\cdot}m^{-1}{\cdot}K^{-1}$, they perform comparably or better than other cement composites with plant-based fibers like date palm, cork, alfa, etc. [6, 15, 49]).

3.2.2. Impact of Relative Humidity (RH)

Fig. 10 represents the evolution of the thermal conductivity at 25°C as a function of RH for the various mortars and allows to better examine the influence of relative humidity level on thermophysical properties. Measurements under dry conditions appear almost similar to those at 50 % RH, while significant increase in thermal conductivity is observed under saturated conditions.

The impact of RH levels is also illustrated in Fig. 11, which shows thermal conductivity versus temperature for mortar M10F containing 6.94 wt% fibers, under different moisture conditions. At 25°C, the thermal conductivity for this M10F specimen is approximately 0.3 $W{\cdot}m^{-1}{\cdot}K^{-1}$ under dry and 50 % RH conditions. However, in a 100 % RH environment, this value increases to approximately 0.6 $W.m^{-1}.K^{-1}$, nearly doubling the dry-state measurement. Despite this increase, the value still falls within the acceptable range for insulation materials. Another noteworthy observation is that the gap in thermal conductivity between dry and

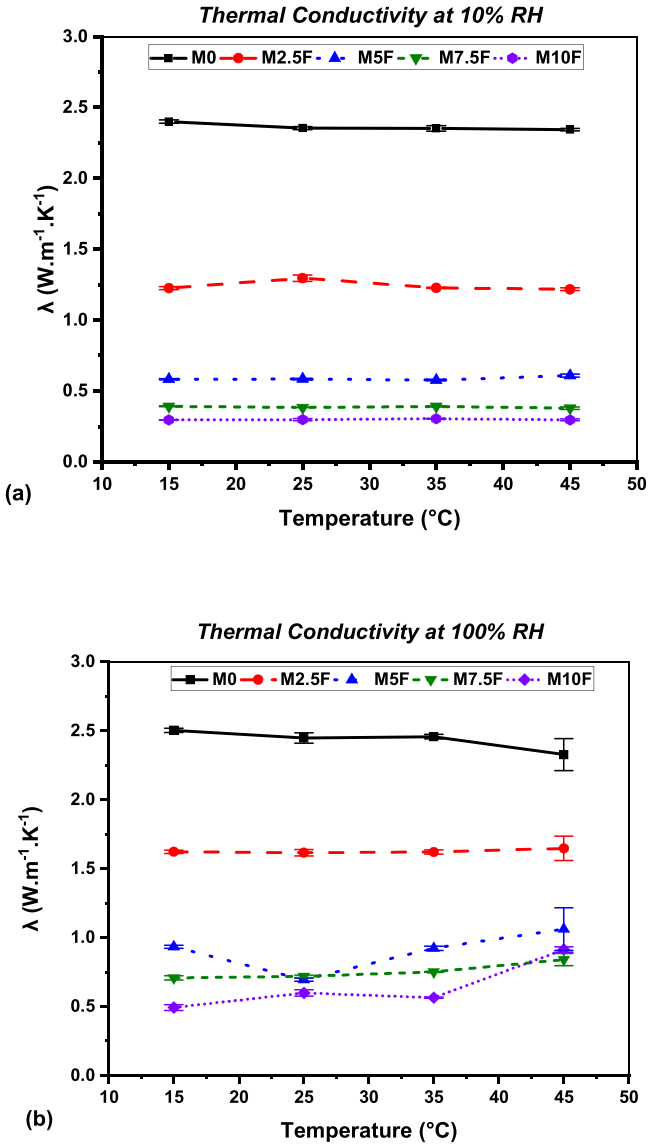

Fig. 8. Temperature dependence of the thermal conductivity at (a) 10 % RH and (b) 100 % RH for the various mortars studied.

saturated states tends to widen as the temperature rises to 45°C.

Several studies support these findings, demonstrating a direct relationship between moisture content and thermal conductivity of bio-based mortars. For instance, Siwińska and Garbalińska [40] reported that higher moisture levels increased conductivity across dry, wet, and moderate conditions for various mortars. Similarly, in the case of hemp concrete, Gourlay et al. [17] reported a 60–75 % rise conductivity from dry to saturated states, while Pierre et al. [18] observed a 50 % increase as RH rose from 0 % to 95 %.

Finally, Fig. 12 presents the thermal conductivity of the biobased mortars at 25°C as a function of miscanthus fiber content, across different RH levels. It clearly shows that the difference in thermal conductivity between dry and saturated states is minimal for the reference mortar but increases significantly with higher fiber content. This effect results from the combined influence of greater mortar porosity (see Section 3.1) and the intrinsic porosity and high water absorbency of miscanthus fibers. In the saturated state, the absorbed water within the micro- and macro-pores enhances heat transfer through the material [17,18,40].

3.3. *Water vapor permeability*

The experimental results for water vapor permeability ($\underline{\delta}$) of the mortars, measured according to EN ISO 12572 [35], are detailed in Table 3. To account for the influence of the air layer between the bottom of the sample and the surface of the solution in the cup, the values were corrected following the method described in Section 2.2.3. The corrected values, denoted as δ_c, are also presented in the table.

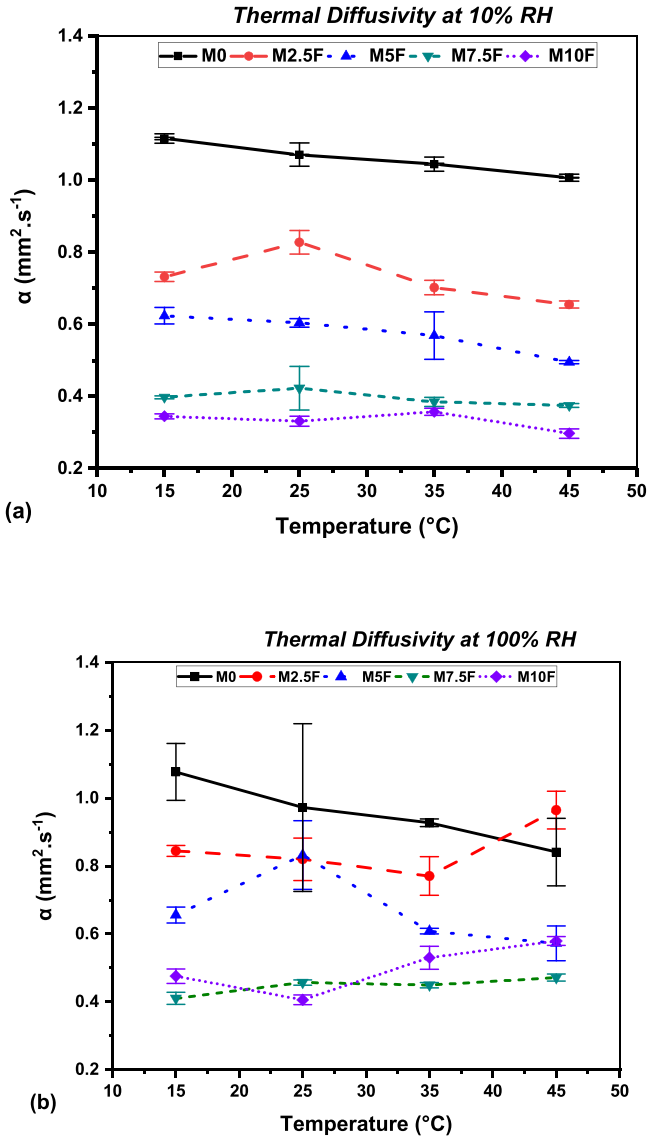

Fig. 9. Temperature dependence of the thermal diffusivity at (a) 10 % RH and (b) 100 % RH for the various mortars studied.

Raw and corrected values of the water vapor resistance factor (μ and μ_c) are also provided in Table 4.

In initial remarks, it is important to highlight that no conclusive values could be established for the reference mortar M0. Indeed, the mass fluctuations of the samples were very slow, and no stabilization could be achieved after several months of test (the standard protocol stipulates that test can be stopped when the deviation between the average value of the 5 last measurements and each individual measurement falls below 5 %, but this criterion was not met in the present case). This is likely due to the very slow kinetics of moisture transfer in this reference material.

It is observed that the water vapor permeability increases with higher fiber content in the mortar matrix. Notably, the mortar composition M10F containing 6.94 wt% of miscanthus fibers demonstrates a water vapor permeability of 1.33×10^{-11} and 2.86×10^{-11} $kg.m^{-1}.s^{-1}.Pa^{-1}$ under dry and wet cup conditions, respectively (after correcting for the air layer effect, the values are 1.91×10^{-11} and 8.43×10^{-11} $kg{\cdot}m^{-1}{\cdot}s^{-1}{\cdot}Pa^{-1}$, respectively). Concurrently, an expected decrease in the water resistance factor is also observed as fiber content increases.

These findings fall within a comparable range to those reported in previous literature on bio-based mortars. For instance, Chennouf et al. [15], who investigated hygrothermal properties of mortars containing 15 wt% date palm fibers, documented water vapor permeability values of 3.16×10^{-11} and 3.59×10^{-11} $kg.m^{-1}.s^{-1}.Pa^{-1}$ for dry cup and wet cup conditions, respectively. Similarly, Benmahiddine et al. [9] reported values of 2.86×10^{-11} and 3.94×10^{-11} $kg.m^{-1}.s^{-1}.Pa^{-1}$ for un-weathered and weathered mortars containing hemp shives. Additionally, Brás et al. [16] observed a 20 % increase in water vapor permeability with the incorporation of 70 % cork into the mortar composition.

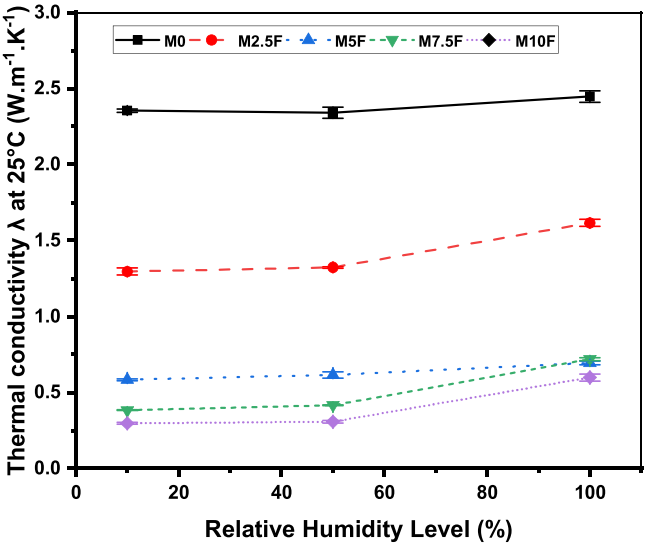

Fig. 10. Dependence of the thermal conductivity of mortars at 25°C upon relative humidity.

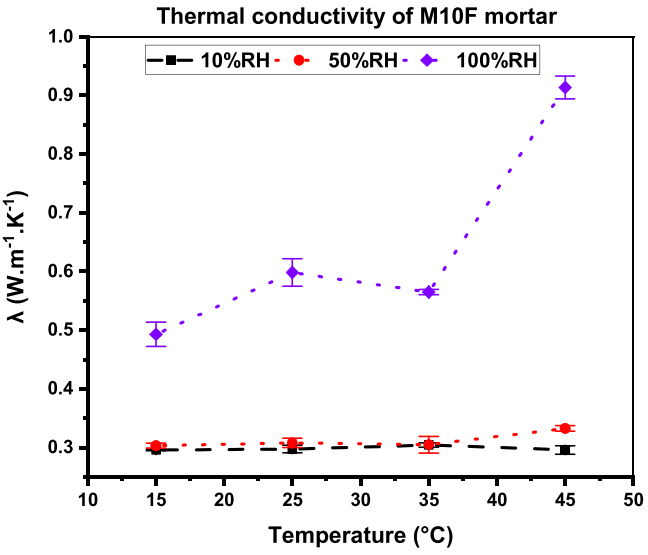

Fig. 11. Dependence of the thermal conductivity of M10F mortar upon temperature, for different levels of relative humidity.

It's worth highlighting that the water vapor permeability exhibits a higher value in the wet cup compared to the dry cup. This difference can be attributed to the enhancement of macroscopic moisture transport within water-filled pores [15,47,48].

Furthermore, the water vapor permeability is closely tied to the microstructure of the mortar. This is significantly affected by the type of binder employed, but more prominently by the fiber content and the dimensions of the fibers integrated into the mortar. The substantial porosity of vegetable fibers promotes enhanced moisture transport capabilities, primarily driving the overall increase in moisture transportation and, consequently, total water vapor permeability [9,15,48,49].

3.4. Sorption/desorption behavior

3.4.1. Experimental characterization

Adsorption and desorption isotherms were determined on the various mortars using the ProUmid SPS apparatus, and following the experimental protocol outlined in Section 2.2.4. These isotherms, depicting the adsorption and desorption characteristics of the studied mortar formulations, are presented in Fig. 13.

Based on these findings, the reference mortar M0 demonstrates a markedly low moisture adsorption capacity, characterized by relatively slow adsorption kinetics. The maximum water adsorption remains below 4 %, reflecting a limited water buffering capacity.

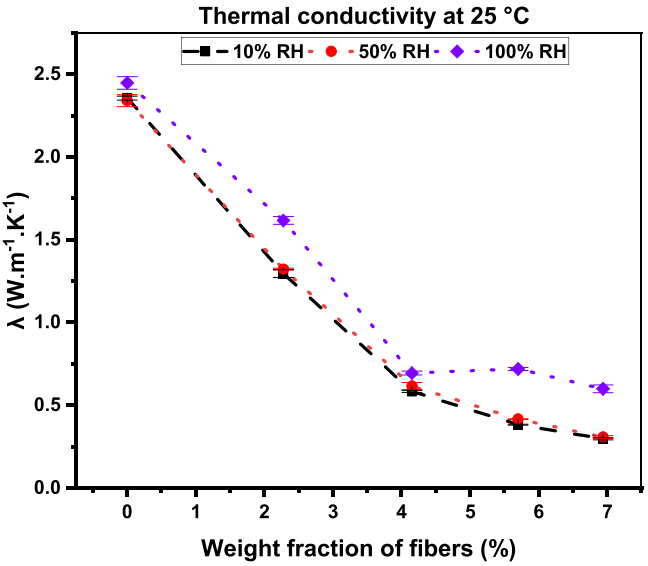

Fig. 12. Dependence of the thermal conductivity of mortars at 25°C upon the weight content of miscanthus fibers, for different levels of relative humidity.

Table 3
Experimental values of water vapor permeability (δ) obtained for the various mortars exposed to dry and wet environments.

Type of mortar	Water vapor permeability (δ) [kg.m^{-1}.s^{-1}.Pa^{-1}] $\times 10^{-11}$		Corrected water vapor permeability (δ_c) [kg.m^{-1}.s^{-1}.Pa^{-1}] $\times 10^{-11}$	
	Dry cup	*Wet cup*	*Dry cup*	*Wet cup*
M0	-	-	-	-
M2.5 F	0.23	0.54	0.24	0.61
M5F	0.48	0.79	0.54	0.97
M7.5 F	1.28	2.48	1.81	5.78
M10F	1.33	2.86	1.91	8.43

Table 4
Experimental values of water vapor resistance factor (μ) obtained for the various mortars exposed to dry and wet environments.

Type of mortar	Water vapor resistance factor (μ)		Corrected water vapor resistance factor (μ_c)	
	Dry cup	*Wet cup*	*Dry cup*	*Wet cup*
M0	-	-	-	-
M2.5 F	86.64	37.67	81.97	33.01
M5F	42.41	25.58	37.74	20.92
M7.5F	15.83	8.16	11.16	3.50
M10F	15.21	7.06	10.54	2.40

This observation is consistent with findings from previous research in the literature [50].

Nevertheless, the introduction of miscanthus fibers into the cementitious matrix yielded a noteworthy enhancement in its hydric behavior. It's evident that the maximum water content adsorbed is correlated to the rate of miscanthus fiber incorporation into the material. A remarkable increase of approximately 104 % and 163 % in maximum adsorbed water content was observed in the M2.5 F and M10F formulations, respectively, when compared to the reference formulation M0. This effect becomes particularly pronounced at relative humidity levels above 65 % RH, where the slope of the adsorption isotherms increases with the fiber content in the biobased mortars. This behavior may be attributed to the additional water-accessible porosity introduced by fiber addition (see Section 3.1), which includes both the intrinsic porosity of the fibers themselves and the porosity formed within the cement matrix and at the interfacial regions between the fibers and the matrix.

Moreover, the experiments reveal that the hysteresis effect between the adsorption and desorption phases increases with fiber content in the biobased mortars, up to 5.7 wt% (mortar M7.5 F), and then seems to stabilize at higher fiber concentration (mortar M10F). This suggests that adding fibers primarily leads to the formation of small pores, promoting an 'ink-bottle' effect [51]. During desorption, large pores begin to empty only after smaller pores have emptied under relatively high capillary pressures. If the necessary capillary pressure is not reached, water may remain trapped in these pores, contributing to the observed widening of the hysteresis

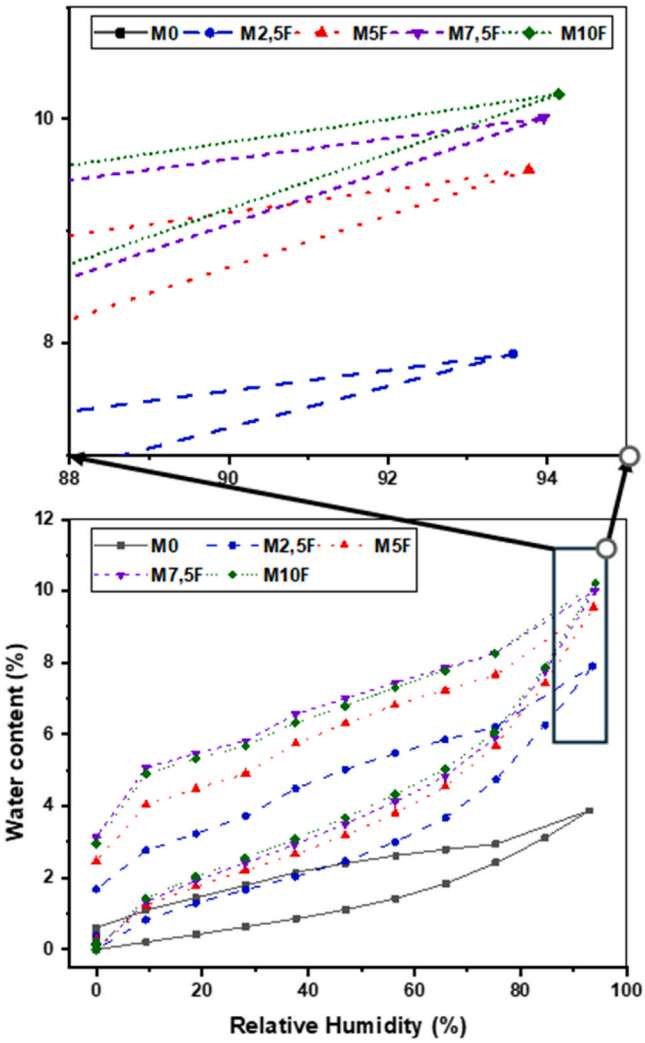

Fig. 13. Adsorption/desorption isotherms recorded for the different mortar formulations.

loops.

Additionally, Fig. 14 depicts the variations in moisture storage capacity in relation to relative humidity levels, as determined from the slopes of the sorption isotherms (as per Eq. (9)). These data underscore a notable enhancement in moisture storage capacity resulting from the incorporation of miscanthus fibers over the entire RH range, although the improvement is more pronounced at high relative humidity levels.

For a specified fiber content, the moisture storage capacity curve exhibits minimal fluctuation within the relative humidity (RH) range of 10–50 %. This observation may account for the near-identical thermophysical properties (specifically, thermal conductivity and thermal diffusivity) observed under both dry (10 % RH) and moderate (50 % RH) humidity conditions for a given mortar, as demonstrated previously in Section 3.2. In contrast, a notable increase in the moisture storage capacity curve becomes evident beyond 65 % RH, which aligns with the higher thermal conductivity values previously obtained under elevated humidity conditions (100 % RH), as compared to low/moderate RH levels.

As revealed by SEM observations (refer to Fig. 1), miscanthus fibers exhibit a highly porous microstructure. This characteristic grants them a remarkable moisture adsorption capacity, consequently enhancing the hygric behavior of the cement composite. A similar phenomenon has been documented in the literature concerning flax concrete, where researchers confirmed improved adsorption capacity with increased incorporation of flax shives [51].

Given the use of a micronized powder in the current study, it's anticipated that a higher surface area will be achieved in comparison to conventional long-chopped fibers [43]. This characteristic is likely a significant factor contributing to the observed improvement in the mortar's moisture absorption capacity compared to the reference material. Unfortunately, this study did not assess the fiber's micropore distribution or specific surface area; these aspects should be explored in future research.

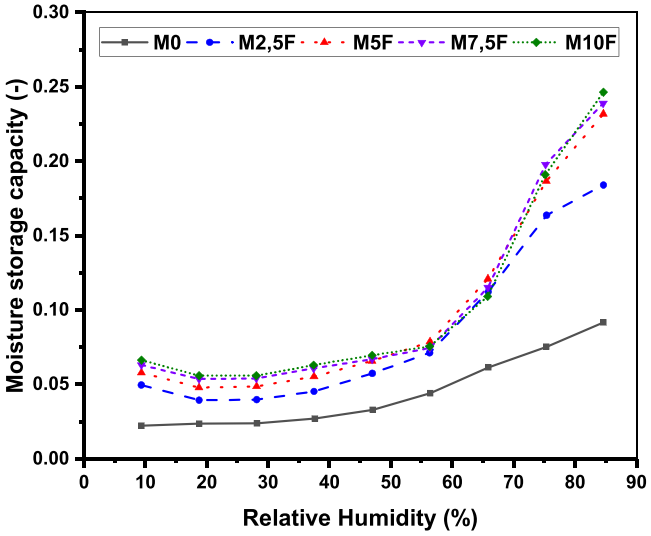

Fig. 14. Moisture storage capacity determined for the different mortar formulations.

3.4.2. *Numerical modeling*

The primary objective of this section is to propose a numerical representation of the experimental sorption behavior, which can serve as input for future modeling of thermo-hydric behavior at the wall scale.

It's worth noting that various models have been developed to predict sorption isotherms, aiming to describe the relationship between the adsorbed solute quantity and either pressure or concentration in the liquid phase. Among these models, the Guggenheim-Anderson-de Boer (GAB) semi-empirical model stands out due to its simplicity and accuracy, particularly for single-layer systems. This model, initially formulated in 1945, has been further enhanced with the introduction of a corrective coefficient k to account for the heat adsorbed by all molecular layers [52,53]. This extension allows for its application across the entire spectrum of relative humidity (as detailed in Eq. (12)). This GAB expression can be easily integrated into numerical models of coupled heat and mass transfer that require sorption characteristic inputs.

$$w = \frac{m.c.k.RH}{(1 - k.RH)(1 - k.RH + k.c.RH))} \tag{12}$$

Where (w) is the equilibrium moisture content, (RH) is the relative humidity, (m) is the monolayer capacity, (c) is a constant related to sorption in the first layer, and (k) is a constant related to multilayer adsorption.

Numerical simulations generated through the GAB model are showcased in Fig. 15 along with experimental data, while the model's fitting parameters are detailed in Table 5. These findings demonstrate the effectiveness of the GAB model in capturing the adsorption isotherm for the experimental dataset, with a minimum correlation coefficient of 0.97 which confirms the robust alignment between the experimental evidence and the model's predictive outcomes.

The Root Mean Square Error (RMSE), as detailed in Table 5, serves as a metric evaluating the accuracy of the prediction model employed in this study. Computed by averaging the squares of the differences between GAB model predictions and experimentally obtained values, the RMSE is derived by taking the square root of this average. This measure reflects the average deviation of predictions from experimental data, presented in the same units as the reference data. Notably, the low RMSE values observed in these results confirm the high reliability of GAB predictions.

3.5. *Moisture buffer value*

Fig. 16 presents the Moisture Buffer values (MBV) of the different mortars obtained according to the NordTest protocol (detailed in Section 2.2.2.), and compares these values with the NordTest Classification [13,14].

The reference mortar, M0, exhibits a notably low MBV value of 0.5 $g.m^{-2}.\%RH^{-1}$, indicating its constrained moisture regulation capabilities, as per the NordTest classification. This observation aligns with earlier findings from vapor permeability and sorption tests, which emphasized slow moisture transfer kinetics in this reference material.

As the proportion of miscanthus fibers in the mortar mix increases, there is a notable enhancement in the MBV. Notably, M5F mortar, containing 4.15 wt% of fibers, exhibits a substantial MBV value of 1.93 $g.m^{-2}.\%RH^{-1}$, thereby qualifying as a good material for moisture buffering. With higher fiber content, the material elevates its performance to an excellent moisture regulator according to the classification; for instance, M10F mortar including 6.94 % of fibers demonstrates an MBV value of 2.05 $g.m^{-2}.\%RH^{-1}$.

A similar trend is consistently observed in numerous studies within the literature on bio-based mortars incorporating various plant fibers such as date palm, hemp, and more, as previously mentioned in the introduction section [9,15,36,49,54].

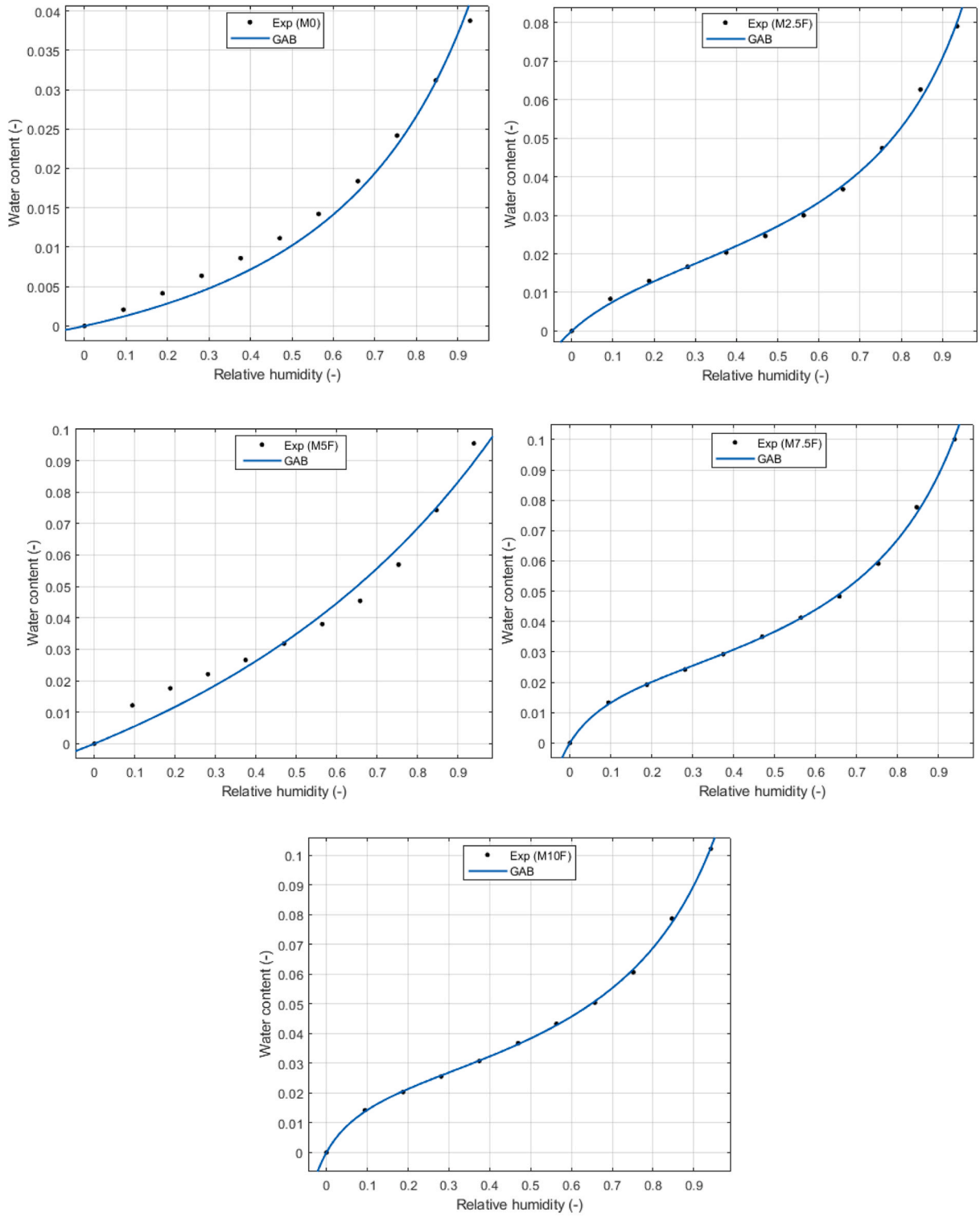

Fig. 15. Comparison of numerical adsorption isotherms provided by the GAB model with experimental data, for the various mortars under study.

This improvement in hygroscopic behavior of bio-based mortar is attributed to the high intrinsic porosity and specific surface area of the vegetal fibers and their good absorptivity [6,9,15,36,49,54]. Additionally, in this work, a good hygroscopic behavior is observed even at low fiber contents, probably due to the use of a micronized miscanthus powder which increases further the specific surface area of fibers.

Table 5
Adjustment parameters for the GAB model.

Type of mortar	Adjustment parameters			R^2	RMSE
	m	k	c		
M0	−0.02287	0.21230	−2.40300	0.9793	0.0017977
M2.5 F	0.02001	0.81520	0.81520	0.9978	0.0012697
M5F	−0.14440	0.06948	−5.26100	0.9717	0.0053145
M7.5F	0.02474	0.81070	11.01000	0.9993	0.0008806
M10F	0.02592	0.80110	11.82000	0.9995	0.0007125

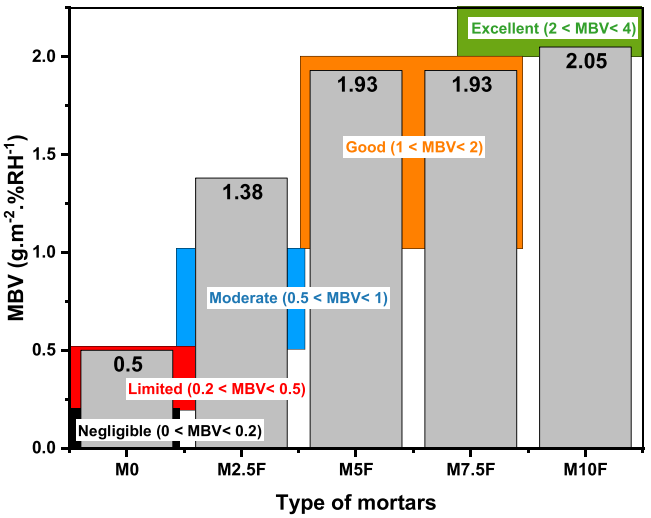

Fig. 16. Moisture Buffer Values of various mortars including miscanthus fibers, and comparison with the NordTest classification.

3.6. Capillary absorption behavior

In contrast to the previous tests that assessed the transport properties of water vapor within the different mortars, the capillary test focuses on characterizing the absorption capacity of the cement composite when it comes into contact with liquid water. These tests were conducted in accordance with the protocol outlined in Section 2.2.5., enabling the determination of both the capillary absorption coefficient (a) and the capillary moisture content (W_f).

Fig. 17 presents the quantity of water absorbed per surface unit versus the square root of time for the various mortar specimens during the capillary absorption test. Capillary absorption parameters (a and W_f) derived from these experiments are reported in Table 6, and their evolutions as a function of the miscanthus fiber content are depicted in Fig. 18.

Regarding the reference mortar M0, we determined a value of 0.023 $kg.m^{-2}.s^{-0.5}$ for the capillary absorption coefficient. This finding is consistent with the results presented by Sicakova et al. [55], who reported a value of 1.92 $kg.m^{-2}.h^{-0.5}$ (equivalent to 0.032 $kg.m^{-2}.s^{-0.5}$) for conventional cement mortar.

When the fiber content in mortar is increased, there is a corresponding increase in the capillary absorption coefficient, reaching a maximum value of 0.13 $kg.m^{-2}.s^{-0.5}$ for M10F mortar containing 6.94 wt% of fibers. This phenomenon can be attributed to the notably high absorptivity of miscanthus fibers. Consistent findings in this regard have also been reported by other researchers. For instance, Page et al. [56] observed for various formulation of concrete containing hemp fibers a water absorption coefficient around 2.52 $kg.m^{-2}.s^{-0.5}$ (equivalent to 0.042 $kg.m^{-2}.s^{-0.5}$). Othmen et al. [57] reported capillary absorption coefficients of 0.16, 0.09, and 0.03 $kg.m^{-2}.s^{-0.5}$ while investigating the capillary absorption behavior of three different hemp concrete. Walker & Pavía [48] obtained capillary absorption coefficients between 0.0495 – 0.0515 $kg.m^{-2}.s^{-0.5}$ for hemp concrete with different binders.

Overall, the capillary absorption coefficient and capillary moisture content of mortars exhibit an upward trend as the fiber content is augmented (up to + 465 % for the absorption coefficient and +223 % for the moisture content in the case of M10F mortar containing 6.94 wt% of fibers, compared to the reference material). This significant increase can be attributed to the high water-absorbing properties of the microporous structure in the cellulose-rich component of miscanthus fibers. Consequently, the biobased mortars show higher absorption of liquid water, resulting in the observed rise in capillary moisture content [48,57–59]. Again, this phenomenon is likely further accentuated by the use of micronized fibers, which are expected to exhibit higher absorptivity compared to long chopped fibers [43].

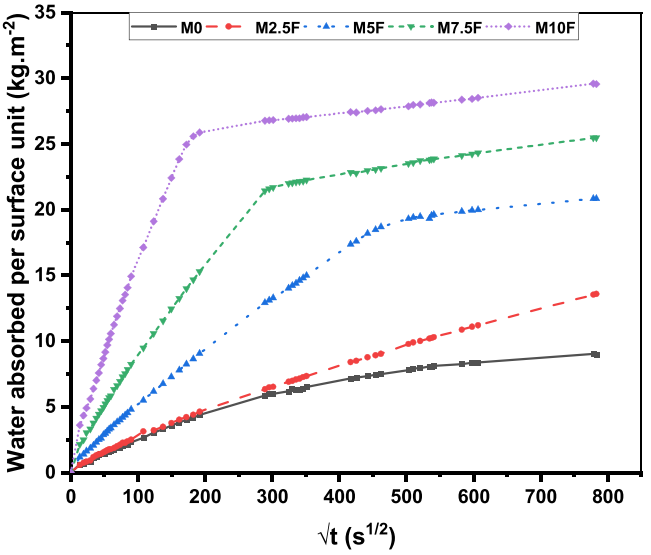

Fig. 17. Evolution of the absorbed water per surface unit during capillary absorption test, for the various mortar specimens.

Table 6
Capillary test results of various mortars.

Type of mortar	Capillary absorption coefficient (a) kg.m^{-2}.s$^{-0.5}$	Capillary moisture content (W_f) kg.m^{-3}
M0	0.023	103.8
M2.5 F	0.025	151.0
M5F	0.048	242.4
M7.5F	0.081	294.4
M10F	0.13	336.2

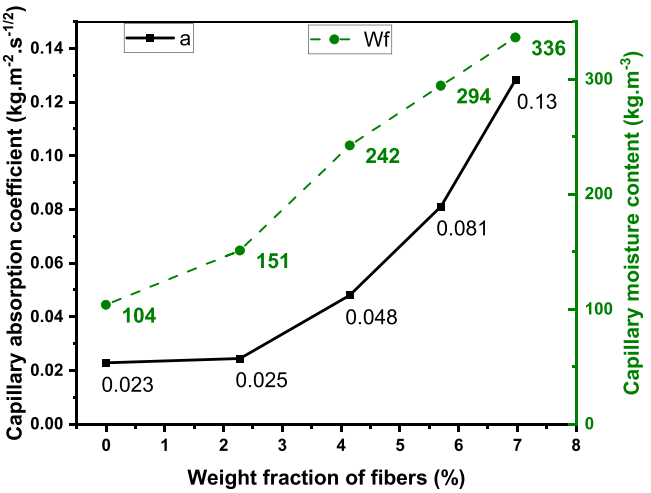

Fig. 18. Evolutions of the capillary absorption coefficient a and the capillary moisture content W_f as a function of the miscanthus fiber content in the cement mortars.

4. Conclusion

This research investigated the hygrothermal properties of cement mortars containing micronized miscanthus fibers at concentrations up to approximately 7 wt%.

In a first step, the study assessed how moisture content variations affected thermal conductivity and diffusivity at different humidity levels (10 % RH, 50 % RH, and 100 % RH). Overall, the results showed that incorporating miscanthus fibers significantly

enhanced thermal resistance, reducing thermal conductivity by 75–80 % compared to the reference mortar due to the fibers' low conductivity and the increased porosity of the mortars. Notably, thermal conductivity was higher in moisture-saturated samples, especially at elevated fiber contents, due to water filling the fibers' microporosities.

Comprehensive hygric characterization revealed that miscanthus fibers deeply modified the moisture-related properties of the biobased mortars, including water vapor permeability, moisture absorption capacity, Moisture Buffer Value (MBV), and capillary absorption. The moisture storage capacity increased with fiber content across all RH levels, with a marked rise beyond 65 % RH, correlating with the higher thermal conductivity observed at 100 % RH. Additionally, GAB fitting provided accurate description of experimental sorption isotherms. Moreover, the MBV of the biobased mortars increased to 2.05 $g{\cdot}m^{-2}{\cdot}\%RH^{-1}$ for the highest fiber content, indicating excellent moisture buffering capacity. Capillary absorption also increased significantly, with the absorption coefficient for M10F mortar rising by up to 465 % compared to the reference material. However, the enhanced hygroscopicity of miscanthus mortars raises concerns about the risk of biodegradation and mold growth, warranting further investigation under varied environmental conditions.

In conclusion, mortars with the higher miscanthus fiber content (M7.5 F and M10F) exhibited remarkable hygroscopicity and low thermal conductivity, highlighting their potential for applications requiring a balance of hygric performance and insulation. The moisture transport coefficients reported in this work provide valuable inputs for future modeling of moisture transfer behavior in cement mortars incorporating miscanthus fibers.

Funding

This research received financial support from the Labex MMCD (Multi-Scale Modelling & Experimentation of Materials for Sustainable Construction), through ANR Investments for the Future (program ANR-11-LABX-022–01).

CRediT authorship contribution statement

Franck Komi Gbekou: Writing – review & editing, Writing – original draft, Visualization, Methodology, Formal analysis, Data curation. **Ferhat Benmahiddine:** Writing – review & editing, Visualization, Methodology, Formal analysis. **Abderrahim Boudenne:** Writing – review & editing, Writing – original draft, Visualization, Supervision, Methodology, Formal analysis. **Rafik Belarbi:** Writing – review & editing, Visualization. **Anissa Eddhahak:** Writing – review & editing, Visualization. **Karim Benzarti:** Writing – review & editing, Writing – original draft, Visualization, Supervision, Project administration, Methodology, Funding acquisition, Formal analysis, Conceptualization.

Declaration of Competing Interest

The authors declare that they have no known competing financial interests or personal relationships that could have appeared to influence the work reported in this paper.

Acknowledgements

The authors would like to acknowledge Vicat Company for providing the OPC and Alpenat cements, and Addiplast Group for supplying the micronized miscanthus fibers.

Appendix. – Complementary tables

Table A1
Densities of the raw materials used in the miscanthus mortar formulations (values provided by the suppliers, except for the miscanthus fibers)

Component	Standard sand	OPC	CSA	SP	Miscanthus fibers
Density (kg m^{-3})	2640	3190	2970	1060	1570*

* Value of the skeleton density of miscanthus reported by Wu et al. [60].

Table A2
Theoretical compositions of the various miscanthus mortars in kg per m^3 of fresh mix. The amount of total water includes water absorbed by miscanthus fibers at pre-soaking stage.

Type of mortar	Sand	OPC	CSA	SP	Miscanthus fibers	Total water
M0	1062	833	63	2.3	0	314
M2.5 F	886	695	52	1.9	48	397
M5F	746	586	44	1.6	80	466

(*continued on next page*)

Table A2 (*continued*)

Type of mortar	Sand	OPC	CSA	SP	Miscanthus fibers	Total water
M7.5F	642	503	38	1.4	103	519
M10F	553	434	33	1.2	118	567

Data availability

Data will be made available on request.

References

[1] International Energy Agency (IEA), Tracking Buildings 2021, Paris, 2021. ⟨https://www.iea.org/reports/tracking-buildings-2021⟩.
[2] Service des données et études statistiques, Bilan énergétique de la France en 2021 - Données provisoires, 2022. ISSN: 2557-8510.
[3] S. Amziane, M. Sonebi, Overview on Biobased Building Material made with plant aggregate, RILEM Tech. Lett. 1 (2016) 31–38, https://doi.org/10.21809/rilemtechlett.2016.9.
[4] J.K. Prusty, S.K. Patro, S.S. Basarkar, Concrete using agro-waste as fine aggregate for sustainable built environment – A review, Int. J. Sustain. Built Environ. 5 (2016) 312–333, https://doi.org/10.1016/j.ijsbe.2016.06.003.
[5] P. Shafigh, H.B. Mahmud, M.Z. Jumaat, M. Zargar, Agricultural wastes as aggregate in concrete mixtures – A review, Constr. Build. Mater. 8 (2014).
[6] M. Charai, A. Mezrhab, L. Moga, M. Karkri, Hygrothermal, mechanical and durability assessment of vegetable concrete mixes made with Alfa fibers for structural and thermal insulating applications, Constr. Build. Mater. 335 (2022) 127518, https://doi.org/10.1016/j.conbuildmat.2022.127518.
[7] M. Boumhaout, L. Boukhattem, H. Hamdi, B. Benhamou, F. Ait Nouh, Thermomechanical characterization of a bio-composite building material: Mortar reinforced with date palm fibers mesh, Constr. Build. Mater. 135 (2017) 241–250, https://doi.org/10.1016/j.conbuildmat.2016.12.217.
[8] O. Horma, M. Charai, S. El Hassani, A. El Hammouti, A. Mezrhab, Thermo-physical and mechanical characterization of cement-based mortar incorporating spent tea, J. Build. Eng. 52 (2022) 104392, https://doi.org/10.1016/j.jobe.2022.104392.
[9] F. Benmahiddine, F. Bennai, R. Cherif, R. Belarbi, A. Tahakourt, K. Abahri, Experimental investigation on the influence of immersion/drying cycles on the hygrothermal and mechanical properties of hemp concrete, J. Build. Eng. 32 (2020) 101758, https://doi.org/10.1016/j.jobe.2020.101758.
[10] D.K. Panesar, B. Shindman, The mechanical, transport and thermal properties of mortar and concrete containing waste cork, Cem. Concr. Compos. 34 (2012) 982–992, https://doi.org/10.1016/j.cemconcomp.2012.06.003.
[11] T. Jami, S.R. Karade, L.P. Singh, A review of the properties of hemp concrete for green building applications, J. Clean. Prod. 239 (2019) 117852, https://doi.org/10.1016/j.jclepro.2019.117852.
[12] T. Colinart, D. Lelievre, P. Glouannec, Experimental and numerical analysis of the transient hygrothermal behavior of multilayered hemp concrete wall, Energy Build. 112 (2016) 1–11, https://doi.org/10.1016/j.enbuild.2015.11.027.
[13] C. Rode, R. Peuhkuri, K.K. Hansen, B. Time, K. Svennberg, J. Arfvidsson, T. Ojanen, NORDTEST Project on Moisture Buffer Value of Materials, (2005) 7.
[14] C. Rode, R. Peuhkuri, B. Time, K. Svennberg, T. Ojanen, P. Mukhopadhyaya, M. Kumaran, S.W. Dean, Moisture buffer value of building materials, J. ASTM Int. 4 (2007) 100369, https://doi.org/10.1520/JAI100369.
[15] N. Chennouf, B. Agoudjil, A. Boudenne, K. Benzarti, F. Bouras, Hygrothermal characterization of a new bio-based construction material: Concrete reinforced with date palm fibers, Constr. Build. Mater. 192 (2018) 348–356, https://doi.org/10.1016/j.conbuildmat.2018.10.089.
[16] A. Brás, F. Gonçalves, P. Faustino, Cork-based mortars for thermal bridges correction in a dwelling: Thermal performance and cost evaluation, Energy Build. 72 (2014) 296–308, https://doi.org/10.1016/j.enbuild.2013.12.022.
[17] E. Gourlay, P. Glé, S. Marceau, C. Foy, S. Moscardelli, Effect of water content on the acoustical and thermal properties of hemp concretes, Constr. Build. Mater. 139 (2017) 513–523, https://doi.org/10.1016/j.conbuildmat.2016.11.018.
[18] T. Pierre, T. Colinart, P. Glouannec, Measurement of Thermal Properties of Biosourced Building Materials, Int J. Thermophys. 35 (2014) 1832–1852, https://doi.org/10.1007/s10765-013-1477-0.
[19] S. Barbhuiya, B. Bhusan Das, A comprehensive review on the use of hemp in concrete, Constr. Build. Mater. 341 (2022) 127857, https://doi.org/10.1016/j.conbuildmat.2022.127857.
[20] F. Collet, S. Pretot, Experimental highlight of hygrothermal phenomena in hemp concrete wall, Build. Environ. 82 (2014) 459–466, https://doi.org/10.1016/j.buildenv.2014.09.018.
[21] F.K. Gbekou, K. Benzarti, A. Boudenne, A. Eddhahak, M. Duc, Mechanical and thermophysical properties of cement mortars including bio-based microencapsulated phase change materials, Constr. Build. Mater. 352 (2022) 129056, https://doi.org/10.1016/j.conbuildmat.2022.129056.
[22] F.K. Gbekou, A. Boudenne, A. Eddhahak, K. Benzarti, Mechanical and thermal properties of cement mortar composites incorporating micronized miscanthus fibers, J. Mater. Res. Technol. 26 (2023) 7649–7664, https://doi.org/10.1016/j.jmrt.2023.09.093.
[23] F.K. Gbekou, A. Boudenne, A. Eddhahak, K. Benzarti, Mechanical and hygrothermal properties of cement mortars including both phase change materials and miscanthus fibers (Cham), in: S. Amziane, I. Merta, J. Page (Eds.), Bio-Based Building Materials, Springer, Nature Switzerland, 2023, pp. 804–816, https://doi.org/10.1007/978-3-031-33465-8_62 (Cham).
[24] F.K. Gbekou, A. Boudenne, A. Eddhahak, K. Benzarti, Comparative Study of the Thermal Behaviors of a Cement Mortar Wall Including Bio-based Microencapsulated Phase Change Materials and a Reference Wall (Cham), in: S. Amziane, I. Merta, J. Page (Eds.), Bio-Based Building Materials, Springer Nature Switzerland, Cham, 2023, pp. 817–828, https://doi.org/10.1007/978-3-031-33465-8_63.
[25] R. Pude, C.-H. Treseler, R. Trettin, G. Noga, Suitability of Miscanthus Genotypes for Lightweight Concrete, Bodenkultur 56 (2005) 61–69.
[26] I. Lewandowski, J. Clifton-Brown, A. Kiesel, A. Hastings, Y. Iqbal, 2- Miscanthus, in: E. Alexopoulou (Ed.), Perennial Grasses for Bioenergy and Bioproducts, Academic Press, 2018, pp. 35–59, https://doi.org/10.1016/B978-0-12-812900-5.00002-3.
[27] I. Lewandowski, A. Heinz, Delayed harvest of miscanthus—influences on biomass quantity and quality and environmental impacts of energy production, Eur. J. Agron. 19 (2003) 45–63, https://doi.org/10.1016/S1161-0301(02)00018-7.
[28] P.P. Dias, D. Waldmann, Optimisation of the mechanical properties of Miscanthus lightweight concrete, Constr. Build. Mater. 258 (2020) 119643, https://doi.org/10.1016/j.conbuildmat.2020.119643.
[29] N. Khalil, G. Aouad, K. El Cheikh, S. Rémond, Use of calcium sulfoaluminate cements for setting control of 3D-printing mortars, Constr. Build. Mater. 157 (2017) 382–391, https://doi.org/10.1016/j.conbuildmat.2017.09.109.
[30] N. Khalil, Formulation et caractérisation chimique et rhéologique des mortiers imprimables en 3D à base de mélanges de ciments Portland et sulfoalumineux, Université de Lille, 2018. ⟨https://tel.archives-ouvertes.fr/tel-02900865/document⟩.
[31] European Committee for Standardization (CEN), NF EN 196-1: Methods of testing cement — Part 1: Determination of strength, (2016).
[32] Y. Chen, Q.L. Yu, H.J.H. Brouwers, Acoustic performance and microstructural analysis of bio-based lightweight concrete containing miscanthus, Constr. Build. Mater. 157 (2017) 839–851, https://doi.org/10.1016/j.conbuildmat.2017.09.161.
[33] O. Onuaguluchi, N. Banthia, Plant-based natural fibre reinforced cement composites: A review, Cem. Concr. Compos. 68 (2016) 96–108, https://doi.org/10.1016/j.cemconcomp.2016.02.014.

[34] European Committee for Standardization (CEN), NF EN ISO 22007-2, Plastics — Determination of thermal conductivity and thermal diffusivity — Part 2: Transient planeheat source (hot disc) method, (2015).
[35] NF EN ISO 12572 - Hygrothermal performance of building materials and products — Determination of water vapour transmission properties — Cup method, (2016).
[36] N. Chennouf, B. Agoudjil, T. Alioua, A. Boudenne, K. Benzarti, Experimental investigation on hygrothermal performance of a bio-based wall made of cement mortar filled with date palm fibers, Energy Build. 202 (2019) 109413, https://doi.org/10.1016/j.enbuild.2019.109413.
[37] NF EN 15801 - Determination of water absorption by capillarity, (2010).
[38] P. Shafigh, I. Asadi, A.R. Akhiani, N.B. Mahyuddin, M. Hashemi, Thermal properties of cement mortar with different mix proportions, Mater. De. ConstrucciónN. 70 (2020) 224, https://doi.org/10.3989/mc.2020.09219.
[39] A. Stolarska, J. Strzałkowski, The thermal parameters of mortars based on different cement type and W/C ratios, Materials 13 (2020) 4258, https://doi.org/10.3390/ma13194258.
[40] A. Siwińska, H. Garbalińska, Thermal conductivity coefficient of cement-based mortars as air relative humidity function, Heat. Mass Transf. 47 (2011) 1077–1087, https://doi.org/10.1007/s00231-011-0772-1.
[41] M. Pomianowski, P. Heiselberg, R.L. Jensen, Full-scale investigation of the dynamic heat storage of concrete decks with PCM and enhanced heat transfer surface area, Energy Build. 59 (2013) 287–300, https://doi.org/10.1016/j.enbuild.2012.12.013.
[42] T. Salem, M. Fois, O. Omikrine-Metalssi, R. Manuel, T. Fen-Chong, Thermal and mechanical performances of cement-based mortars reinforced with vegetable synthetic sponge wastes and silica fume, Constr. Build. Mater. 264 (2020) 120213, https://doi.org/10.1016/j.conbuildmat.2020.120213.
[43] N. Benmansour, B. Agoudjil, A. Gherabli, A. Kareche, A. Boudenne, Thermal and mechanical performance of natural mortar reinforced with date palm fibers for use as insulating materials in building, Energy Build. 81 (2014) 98–104, https://doi.org/10.1016/j.enbuild.2014.05.032.
[44] T. Schnabel, H. Huber, A. Petutschnigg, A. Jäger, Analysis of plant materials pre-treated by steam explosion technology for their usability as insulating materials, Agron. Res. 17 (2019) 1191–1198, https://doi.org/10.15159/AR.19.061.
[45] Z. Li, X. Wang, L. Wang, Properties of hemp fibre reinforced concrete composites, Compos. Part A: Appl. Sci. Manuf. 37 (2006) 497–505, https://doi.org/10.1016/j.compositesa.2005.01.032.
[46] M. Chikhi, B. Agoudjil, A. Boudenne, A. Gherabli, Experimental investigation of new biocomposite with low cost for thermal insulation, Energy Build. 66 (2013) 267–273, https://doi.org/10.1016/j.enbuild.2013.07.019.
[47] F. Collet, J. Chamoin, S. Pretot, C. Lanos, Comparison of the hygric behaviour of three hemp concretes, Energy Build. 62 (2013) 294–303, https://doi.org/10.1016/j.enbuild.2013.03.010.
[48] R. Walker, S. Pavía, Moisture transfer and thermal properties of hemp–lime concretes, Constr. Build. Mater. 64 (2014) 270–276, https://doi.org/10.1016/j.conbuildmat.2014.04.081.
[49] B. Haba, B. Agoudjil, A. Boudenne, K. Benzarti, Hygric properties and thermal conductivity of a new insulation material for building based on date palm concrete, Constr. Build. Mater. 154 (2017) 963–971, https://doi.org/10.1016/j.conbuildmat.2017.08.025.
[50] F. Boukhelf, R. Cherif, A. Trabelsi, R. Belarbi, M. Bachir Bouiadjra, On the hygrothermal behavior of concrete containing glass powder and silica fume, J. Clean. Prod. 318 (2021) 128647, https://doi.org/10.1016/j.jclepro.2021.128647.
[51] F. Benmahiddine, R. Cherif, F. Bennai, R. Belarbi, A. Tahakourt, K. Abahri, Effect of flax shives content and size on the hygrothermal and mechanical properties of flax concrete, Constr. Build. Mater. 262 (2020) 120077, https://doi.org/10.1016/j.conbuildmat.2020.120077.
[52] P.P. Lewicki, The applicability of the GAB model to food water sorption isotherms, Int. J. Food Sci. Technol. 32 (1997) 553–557, https://doi.org/10.1111/j.1365-2621.1997.tb02131.x.
[53] W. Wolf, W.E.L. Spiess, G. Jung, H. Weisser, H. Bizot, R.B. Duckworth, The water-vapour sorption isotherms of microcrystalline cellulose (MCC) and of purified potato starch. Results of a collaborative study, J. Food Eng. 3 (1984) 51–73, https://doi.org/10.1016/0260-8774(84)90007-4.
[54] B.K. Kreiger, W.V. Srubar, Moisture buffering in buildings: A review of experimental and numerical methods, Energy Build. 202 (2019) 109394, https://doi.org/10.1016/j.enbuild.2019.109394.
[55] A. Sicakova, M. Draganovska, M. Kovac, Water Absorption Coefficient as a Performance Characteristic of Building Mixes Containing Fine Particles of Selected Recycled Materials, Procedia Eng. 180 (2017) 1256–1265, https://doi.org/10.1016/j.proeng.2017.04.287.
[56] J. Page, M. Sonebi, S. Amziane, Design and multi-physical properties of a new hybrid hemp-flax composite material, Constr. Build. Mater. 139 (2017) 502–512, https://doi.org/10.1016/j.conbuildmat.2016.12.037.
[57] I. Othmen, P. Poullain, N. Leklou, Capillary action in three hemp concretes, (2014). https://doi.org/DOI 10.3233/978-1-61499-466-4-1358.
[58] A. Ruus, T. Koosapoeg, M. Pau, T. Kalamees, M. Põldaru, Influence of production on hemp concrete hygrothermal properties: sorption, water vapour permeability and water absorption, J. Phys.: Conf. Ser. 2069 (2021) 012004, https://doi.org/10.1088/1742-6596/2069/1/012004.
[59] J. Page, M. Sonebi, S. Amziane, Experimental investigation on the performance of hybrid hemp- flax composite materials, First International Conference on Bio-Based Building Materials, AJCE Special Issue 33 (2015).
[60] F. Wu, Q. Yu, H.J.H. Brouwers, Effects of treated miscanthus on performance of bio-based cement mortar, J. Sustain. Cem. -Based Mater. 12 (2023) 357–368, https://doi.org/10.1080/21650373.2022.2059794.